Ions in crystals: The topology of the electron density in ionic materials. II. The cubic alkali halide perovskites

Víctor Luaña, Aurora Costales, and A. Martín Pendás
Departamento de Química Física y Analítica, Facultad de Química, Universidad de Oviedo, E-33006 Oviedo, Spain
(Received 14 December 1995; revised manuscript received 10 October 1996)

We present here the topological (Bader) analysis of the electronic structure for 120 cubic perovskites AMX_3 (A denotes Li, Na, K, Rb, Cs; M denotes Be, Mg, Ca, Sr, Ba, Zn; X denotes F, Cl, Br, I). The perovskite being perhaps the simplest and most abundant structure for ternary compounds, we have found up to seven different topological schemes for the electronic density. Those schemes can be simply arranged and explained in terms of ratios of topologically defined ionic radii. However, no set of empirical radii, even of best-fitted radii, can accomplish the same objective. All crystals do present M-X and A-X bonds, many have X-X too, and only $CsSrF_3$ and $CsBaF_3$ have A-A bonds. The topology and geometry of the electronic density has been further analyzed by depicting the shape of the attraction basins of the ions. Basins have polyhedral shapes and can be simply predicted, in most cases, after the knowledge of the bonds that the ion forms. M^{2+} basins do present, however, bizarre nearly bidimensional wings on those topological schemes lacking X-X bonds. Lattice energy has been found to be dominated by Coulombic interactions and determined by the crystal size more than by the electronic topological scheme, although the influence of the electronic density at the M-X bond critical point is also observed. The stability of the perovskite structure with respect to the decomposition into MX_2+AX has been found to be mostly governed by the M^{2+} cation, the crystals having small M^{2+} and large A^+ ions being the most stable ones. There is also a clear tendency for the crystals lacking X-X bonds, and having bizarre M^{2+} shapes, to decompose. [S0163-1829(97)09204-7]

I. INTRODUCTION

We present a systematic analysis of the topological properties of the electronic density in a family of ionic crystals: the halide perovskites AMX_3. Our analysis lies within the framework of the *atoms in molecules* (AIM) theory developed by Bader and co-workers.[1,2] AIM theory provides a rigorous quantum-mechanical foundation to key concepts of the chemical structure, such as which bonds do exist, how the shape of an atom is and what is its charge, or how the properties of a functional group change from compound to compound. Although it has been extensively applied to a number of organic gas-phase molecules, not many studies have been published concerning solid-state systems.[3–9]

Johnson[10] first suggested using the critical points of the electronic density (ρ) of crystals to help in the analysis of x-ray diffraction patterns. Eberhart *et al.*[5–7] have used AIM theory in the analysis of the electronic density of metals and alloys, defining basic polyhedral forms for bcc alloys and examining the relationship among topological and thermodynamical properties. A similar account of the electronic density topology in bcc lattices of Li and Na has been given by Mei *et al.*[8] Bader's own group has discussed recently some of the consequences of AIM theory as applied to crystals,[3,4] particularly the possibility of defining such structural concepts as the Wigner-Seitz cell of a crystal in terms of the topology of ρ.

On the other hand, to our knowledge, the complete characterization of the topological properties of the electronic density in a solid has not been done before, partly because of the great difficulty in determining all critical points (CP's) and integrating over the atomic basins using the available methodology.[11]

In a previous work[12] we have discussed the extension of AIM theory to solids. It was shown there that several important differences appear, from the point of view of this theory, between gas-phase molecules and solids:

(1) Atomic basins in solids have well-defined boundaries and encompass a finite volume; (2) whereas ring and cage critical points are rare in most small molecules, they are guaranteed to exist and are, in fact, quite abundant in solids; (3) as a consequence of the above, the traditional molecular graph of a solid can be very complicated and, what is more important, it gives only a very poor image of the topological properties of the electronic density.

Many of the topological features exhibited by crystalline solids are, on the other hand, enforced by the point-group and translational symmetry.[12]

We also presented in Ref. 12 an automatic algorithm for the systematic determination of CP's, a technical innovation that opens up the possibility of investigating the relationship between geometry, electronic density topology, and structural stability in a collection of closely related crystals.

In this paper we explore the topological properties of 120 alkali-halide perovskites AMX_3 (A denotes Li, Na, K, Rb, Cs; M denotes Be, Mg, Ca, Sr, Ba, Zn; X denotes F, Cl, Br, I). Our first objective in examining a large family of closely related compounds is to determine whether all these crystals are homeomorphic or, on the contrary, they present a large variety of topological structures.

Another very significant objective is to determine the connections between the electronic density topology and the chemical and structural stability of the compounds. This connection has been repeatedly proposed in the literature, and it has been numerically explored in isolated molecules.[1] Alkali-halide perovskites are very convenient for this pur-

pose. They have a simple crystallographic structure, which facilitates the theoretical calculation of the electronic density as well as the topological analysis. Perovskites, on the other hand, have a rich variety of structural phase transitions and an interesting chemical reactivity.

In addition, even though a rich body of literature exists on the alkali-halide perovskites, both from the experimental and theoretical points of view, a systematic search reveals that most of the possible compounds have never been reported, either as actually being synthesized or as being unstable. The *ab initio* calculations presented and discussed in this paper may contribute to fill in a significant gap in the knowledge of ionic perovskites.

The paper is organized as follows. The computational procedure is presented in Sec. II. Section III contains a detailed description of the most relevant results and it is divided into five parts devoted to (a) introducing the topological structures found on the perovskites; (b) analyzing those structures from a geometrical point of view; (c) discussing the reasons behind the occurrence of different topologies; (d) determining the most relevant ionic properties; and (e) examining some significant correlations between the lattice energy, the geometry, and the topology of the crystal. Finally, in Sec. IV we discuss the meaning and significance of the above results and analyze the relationship between topology and stability.

II. COMPUTATIONAL SCHEME

To begin the analysis of the electronic density we need to know the equilibrium geometry of the compounds. Experimental geometries are not available for most of the perovskites analyzed in this work. As a consequence, we have proceeded by determining, as a first step, the theoretical equilibrium geometry of every crystal. To this end we have done *ab initio* perturbed ion[13,14] (*ai*PI) calculations on all the compounds.

*ai*PI is a quantum-mechanical method that solves the Hartree-Fock equations of a solid in a localized Fock space by partitioning the crystal wave function into local, weakly overlapping, group functions, each containing a number of electrons but a single nucleus.[13,14] The method brings together[15] ideas from the electron separability theory of McWeeny[16] and Huzinaga[17] and from the theory of localizing potentials of Adams[18] and Gilbert[19] to produce a well founded and very efficient treatment for ionic materials.

The *ai*PI method has been successfully applied to the description of a variety of electronic, energetic, and structural properties of ionic crystals, including halides,[13,20–22] simple and complex oxides,[23–26] and sulfides.[27]

The *ai*PI calculations in the present work have been done using the best available Slater-type function (STO) basis sets for all ions.[28] The unrelaxed hard Coulomb hole formalism (uCHF) has been used to estimate the correlation energy,[29] but the crystal wave function has been obtained at the Hartree-Fock level, not being modified by the correlation estimation procedure.[23] All Coulomb interactions have been integrated exactly. Interionic exchange and lattice projection operators, on the other hand, have been accounted for in neighbors up to 25 bohr away.

The perovskite structure [cubic, $Pm\bar{3}m$, A^+ at $(\frac{1}{2},\frac{1}{2},\frac{1}{2})$, M^{2+} at (0,0,0), and X^- at $(\frac{1}{2},0,0)$] fixes all geometrical parameters but one: the cell side length a. We have optimized a for all 120 compounds using a simplex method.

TABLE I. Equilibrium properties of a sample of the 120 perovskites: lattice parameter (a in Å), bulk moduli (B in GPa), and lattice energy (E_{latt} in kcal/mol).

Crystal	a	E_{latt}	B	Expt. a	Expt.
$NaMgF_3$	3.836	−951.97	87.999	3.833	Ref. 61
$KMgF_3$	3.943	−934.77	82.692	3.989	Ref. 73
$RbCaF_3$	4.483	−825.07	47.275	4.431	Ref. 45
$CsCaF_3$	4.459	−830.34	44.147	4.505	Ref. 74
$NaZnF_3$	3.791	−984.30	89.764	3.884	Ref. 75
$KZnF_3$	3.897	−965.80	85.485	4.035	Ref. 74
$RbZnF_3$	3.900	−970.97	86.921	4.110	Ref. 73
$KMgCl_3$	4.998	−737.96	33.849	4.998	Ref. 76
$CsCaCl_3$	5.563	−673.35	23.386	5.396	Ref. 76

The equilibrium properties of a sample of 120 compounds, those perovskites for which reliable experimental geometry of the cubic phase exists, are collected in Table I. More extensive tables are available upon request. Our theoretical geometries are found to agree within 1.1% with these experimental values. The largest discrepancies are found on the Cs crystals, and can be related to the degradation of the hard Coulomb hole functional parameters for the heaviest elements. Previous analyses on alkali and alkaline earth halides indicate that a more realistic estimation of the relative errors of the uCHF *ai*PI calculations to the experimental equilibrium properties is 2–4%, 3–6%, and 10–15% for the lattice parameters, binding energies, and isothermal bulk moduli, respectively.

The ionic wave functions obtained from a final *ai*PI calculation at the optimal geometry have been used in the CRITIC program[30] to determine the crystal wave function for each crystal. Ions up to 3 cell side lengths contributed to the wave function at any point.

The new algorithm designed to automatically find and classify all critical points of a crystal[12] has been found to work remarkably well in most crystals. Early runs that included an insufficient number of ions in the evaluation of the wave function were unable to locate all CP's in some crystals. Once this problem was solved, the only failures of the automatic procedure were (a) false positives of points that showed rather large gradients and that were easily discarded by inspection, and (b) remarkably, the Wyckoff's $3c$ position, which is a CP fixed by symmetry (see below), was considered doubtful in some crystals by the automatic discarding criteria. Morse relationships and similarities among compounds have been analyzed to make sure that all CP's were found in every case.

III. RESULTS

A. Topological structure of the electronic density

It has been discussed in paper I[12] that site symmetry determines that some special positions of the cell *must* be CP's of the electronic density. This is the case for Wyckoff's $1a$, $1b$, $3c$, and $3d$ positions in the $Pm\bar{3}m$ space group of

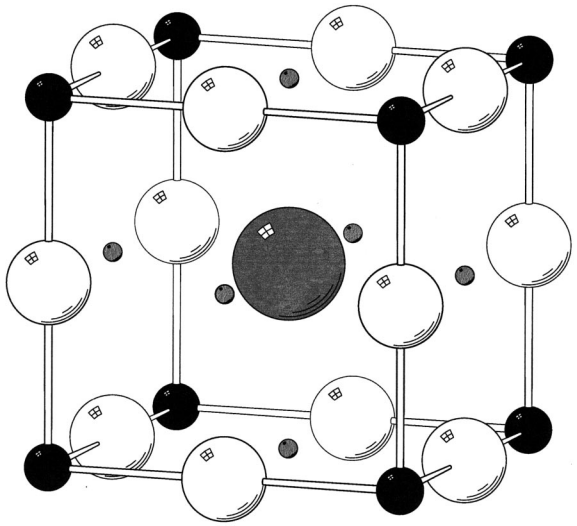

FIG. 1. Scheme of the perovskite unit cell. Ions are represented as: black (M^{2+}), large white (X^-), and large light gray (A^+) balls. Wyckoff's $3c$ position, lying at the center of each cube face, is also represented as small gray balls. This figure has been plotted with MOLSCRIPT (Ref. 77).

the perovskites. Three of these positions are occupied by the crystal ions: A^+ occupies $1b$, M^{2+} $1a$, and X^- $3d$. The $3c$ positions lie at the center of the unit-cell cubic faces, octahedrically surrounded by four equatorial X^- ions and two axial A^+ ions (see Fig. 1), and they play a very important role in determining the overall topology of the electronic density.

After analyzing all 120 halide perovskites we have found that the electronic density can be classified into one of seven different *topological schemes* (i.e., seven different arrangements of critical points). Seven may appear to be a large number for a group of apparently quite similar compounds. On the other hand, we have performed some numerical experiments by placing two-electron imaginary ions, represented as single $1s$ Slater-type orbitals, at the ionic sites. By independently varying the three orbital exponents, we were able to generate a rather large number of topological schemes, including the seven actually obtained for the halide perovskites. This numerical experiment proved that the physical limitation of the ionic sizes effectively reduces to a large extent the possible topological schemes.

The seven topological schemes can be further organized into three families according to the character of Wyckoff's $3c$ position: (a) $3c$ is a bond CP in the $\mathcal{B}$ family; (b) a ring point in the $\mathcal{R}$ family; and (c) a cage point in the $\mathcal{C}$ family. The $\mathcal{B}$ family, which includes only one scheme, is described in Table II, and the $\mathcal{R}$ and $\mathcal{C}$ families, including three different topological schemes each, have been summarized in Table III.

The translationally invariant crystals are topologically equivalent to S^3, the 3-torus, and, consequently, all topological schemes must satisfy Morse invariant relationships:[31,32]

$$n-b+r-c=0, \tag{1}$$

and

$$n\geqslant 1, \quad b\geqslant 3, \quad r\geqslant 3, \quad c\geqslant 1, \tag{2}$$

TABLE II. Topological schemes of CP's of the electronic density found on cubic halide perovskites. The space group is $Pm\bar{3}m$. Float numbers in parentheses represent the x, y, and z coordinates not fixed by symmetry. CP's are listed as: nuclei (n), bonds (b), rings (r), and cages (c), with numerical indexes to distinguish the different types within each kind.

Wyckoff	Symmetry	Symmetry	Position	$CsSrF_3$
$1a$	O_h	$m\bar{3}m$	(0,0,0)	n: Sr
$1b$	O_h	$m\bar{3}m$	$(\frac{1}{2},\frac{1}{2},\frac{1}{2})$	n: Cs
$3c$	D_{4h}	$4/mm.m$	$(0,\frac{1}{2},\frac{1}{2})$	b_4
$3d$	D_{4h}	$4/mm.m$	$(\frac{1}{2},0,0)$	n: F
$6e$	C_{4v}	$4m.m$	$(x,0,0)$	b_1: (0.73171)
$6f$	C_{4v}	$4m.m$	$(x,\frac{1}{2},\frac{1}{2})$	
$8g$	C_{3v}	$.3m$	(x,x,x)	c_2: (0.77150)
$12h$	C_{2v}	$mm2..$	$(x,\frac{1}{2},0)$	r_5: (0.52152)
$12i$	C_{2v}	$m.m2$	$(0,x,x)$	c_5: (0.52581)
$12j$	C_{2v}	$m.m2$	$(\frac{1}{2},x,x)$	b_2: (0.77826)
$24k$	C_s	$m..$	$(0,y,z)$	
$24l$	C_s	$m..$	$(\frac{1}{2},y,z)$	
$24m$	C_s	$..m$	(x,x,z)	r_1: $\begin{pmatrix}0.70679\\0.87703\end{pmatrix}$
$48n$	C_1	1	(x,y,z)	
		$(\tau_n\tau_b\tau_r\tau_c)$ index		3322
		Number of critical points (τ)		10
		Family		$\mathcal{B}$

where n represents the total number of nuclei in the unit cell, b the number of bonds, r the number of rings, and c the number of minima or cages. On the other hand, it is useful to consider τ_n, the number of symmetrically different nuclei in the unit cell, and similarly τ_b, τ_r, and τ_c, the number of symmetrically different bond, ring, and cage points, respectively. The topological schemes can be easily organized in terms of the $\vec{\tau}=(\tau_n,\tau_b,\tau_r,\tau_c)$ vector or, even simpler, by the total number of symmetrically different CP's:

$$\tau=\tau_n+\tau_b+\tau_r+\tau_c\,. \tag{3}$$

All topological schemes found for the perovskites can be uniquely identified by giving the family and value of τ. Furthermore, every scheme has a different τ, except $\mathcal{B}_{10}$ and $\mathcal{C}_{10}$ (to designate each scheme we will give the family as a capital letter and the value of τ as a subindex).

A single scheme, $\mathcal{B}_{10}$, forms the $\mathcal{B}$ family. The scheme presents three different bond CP's: b_4, b_1, and b_2, corresponding to A-A, M-X, and A-X bonds, respectively. The existence of the A-A bond is the most distinctive aspect of the $\mathcal{B}_{10}$ scheme, and it is the consequence of two combined factors: a very large A to X size ratio, and a large cell side length a due to the large size of M. This is an unusual combination and, consequently, only two out of the 120 crystals belong to this scheme: $CsSrF_3$ and $CsBaF_3$.

The $\mathcal{C}$ family comprises three topological schemes, all of them having an even number of different CP's: $\mathcal{C}_8$, $\mathcal{C}_{10}$, and $\mathcal{C}_{12}$. The $\mathcal{R}$ family also shows three topological schemes, all of them having an odd number of different CP's: $\mathcal{R}_9$, $\mathcal{R}_{11}$, and $\mathcal{R}_{13}$. Both families maintain a close relationship and

TABLE III. Topological schemes of CP's of the electronic density found on cubic halide perovskites. The space group is $Pm\bar{3}m$. Float numbers in parentheses represent the x, y, and z coordinates not fixed by symmetry. CP's are listed as nuclei (n), bonds (b), rings (r), and cages (c), with numerical indexes to distinguish the different types of each kind. Only one example crystal is given for each scheme.

Wyckoff	Symmetry	Position	$KCaF_3$	$LiCaF_3$	$KMgF_3$	$LiZnCl_3$	$CsBeI_3$	$LiBeI_3$
$1a$	O_h	(0,0,0)	n: Ca	n: Ca	n: Mg	n: Zn	n: Be	n: Be
$1b$	O_h	$(\frac{1}{2},\frac{1}{2},\frac{1}{2})$	n: K	n: Li	n: K	n: Li	n: Cs	n: Li
$3c$	D_{4h}	$(0,\frac{1}{2},\frac{1}{2})$	c_1	r_2	c_1	r_2	c_1	r_2
$3d$	D_{4h}	$(\frac{1}{2},0,0)$	n: F	n: F	n: F	n: Cl	n: I	n: I
$6e$	C_{4v}	$(x,0,0)$	b_1: (0.25445)	b_1: (0.25559)	b_1: (0.22213)	b_1: (0.22038)	b_1: (0.13463)	b_1: (0.13509)
$6f$	C_{4v}	$(x,\frac{1}{2},\frac{1}{2})$		c_3: (0.20197)		c_3: (0.23265)		c_3: (0.26445)
$8g$	C_{3v}	(x,x,x)	c_2: (0.25066)	c_2: (0.34028)	c_2: (0.24150)	c_2: (0.35535)	c_2: (0.27455)	c_2: (0.37188)
							r_4: (0.16679)	r_4: (0.16666)
							c_4: (0.08807)	c_4: (0.08826)
$12h$	C_{2v}	$(x,\frac{1}{2},0)$						
$12i$	C_{2v}	$(0,x,x)$			r_3: (0.20911)	r_3: (0.77770)	r_3: (0.10345)	r_3: (0.10373)
					b_3: (0.24479)	b_3: (0.76637)	b_3: (0.24976)	b_3: (0.24963)
$12j$	C_{2v}	$(\frac{1}{2},x,x)$	b_2: (0.24537)	b_2: (0.31656)	b_2: (0.24340)	b_2: (0.66772)	b_2: (0.26205)	b_2: (0.34970)
$24k$	C_s	$(0,y,z)$						
$24l$	C_s	$(\frac{1}{2},y,z)$						
$24m$	C_s	(x,x,z)	r_1: $\begin{pmatrix}0.32841\\0.83772\end{pmatrix}$	r_1: $\begin{pmatrix}0.38094\\0.28459\end{pmatrix}$	r_1: $\begin{pmatrix}0.67250\\0.15774\end{pmatrix}$	r_1: $\begin{pmatrix}0.60936\\0.69410\end{pmatrix}$	r_1: $\begin{pmatrix}0.34490\\0.19529\end{pmatrix}$	r_1: $\begin{pmatrix}0.40185\\0.32886\end{pmatrix}$
$48n$	C_1	(x,y,z)						
$(\tau_n\tau_b\tau_r\tau_c)$ index			3212	3222	3322	3332	3333	3343
Number of critical points (τ)			8	9	10	11	12	13
Family			$\mathcal{C}$	$\mathcal{R}$	$\mathcal{C}$	$\mathcal{R}$	$\mathcal{C}$	$\mathcal{R}$

exhibit identical mechanisms in going from the simplest to the most complex scheme. Accordingly, $\mathcal{C}_{10}$ and $\mathcal{R}_{11}$ schemes are obtained from the $\mathcal{C}_8$ and $\mathcal{R}_9$ ones, respectively, by adding both a bond and a ring point at Wyckoff's $12i$ position. Adding up to this both a ring and a cage point at $8g$ position originates the $\mathcal{C}_{12}$ and $\mathcal{R}_{13}$ schemes.

We see here a simple mechanism for increasing the complexity of a topological scheme: add new CP's in pairs, each new point being of a type with different sign in the Morse sum. Either bonds and rings, or rings and cages would do the trick. If both types of CP's appear in the same Wyckoff's position, or in two positions with identical multiplicity, the invariance required by the Morse relation is automatically fulfilled.

The $\mathcal{C}_8$ and $\mathcal{R}_9$ schemes, the simplest in their respective families, present just two types of bond CP's. The bond in Wyckoff's $6e$ position lies at the edges of the cubic unit cell and constitutes a bond between the divalent metal and the halide: M-X. The bond point in $12j$, on the other hand, represents an A-X bond. The other four schemes of the $\mathcal{C}$ and $\mathcal{R}$ families have, in addition, an X-X bond occupying the $12i$ position.

We see that the topological analysis indicates a bonding scheme more complicated than is usually assumed for simple inorganic crystals. Anion-anion bonds, in particular, may appear rather unconventional. It is interesting to mention, in this regard, the predecessor of Pauling, who considered the existence of X-X bonds in some alkali halides as a way to explain the anomalous sequence of geometries observed in LiCl, LiBr, and LiI.[33]

The $\mathcal{R}$ family is the most frequent, and both families, $\mathcal{R}$ and $\mathcal{C}$, show a decreasing number of crystals in passing from the simplest to the most complex topological scheme. The actual number of crystals belonging to each scheme is 21 ($\mathcal{C}_8$), 27 ($\mathcal{R}_9$), 15 ($\mathcal{C}_{10}$), 25 ($\mathcal{R}_{11}$), 12 ($\mathcal{C}_{12}$), and 18 ($\mathcal{R}_{13}$).

B. Analysis of the molecular graphs

Visualizing the arrangements of critical points and the connections among them is not an easy task, given the huge number of points that lie within the unit cell (from 58 CP's in the $\mathcal{C}_8$ scheme to 104 CP's in the $\mathcal{R}_{13}$). The most significant and comprehensive way that we have found is based on depicting the attraction basins for each nuclei, together with its polyhedral approximation: the weighted proximity polyhedra (WPP).

The attraction basin of a nucleus is made out of all the points of space such that a trajectory that starts at the point and moves upward in the gradient field of the electronic density ends in the nucleus. All CP's that, in any way, are related to a nucleus lie at the surface of its attraction basin. The attraction basin has faces, edges, and vertices, which correspond to bond, ring, and cage points, respectively. It is common for the faces to be planar and for the edges to be linear, but this is not always the case and large curvatures do appear in some basins.

Physicists and chemists tend to think of atoms in molecules as slightly deformed spheres. Spheres, however, do not fill the three-dimensional space without gaps and are thus inappropriate approximations to the attraction basins shape in crystals. Polyhedra do represent a better approach, but we have to keep in mind that in passing from curved faces and

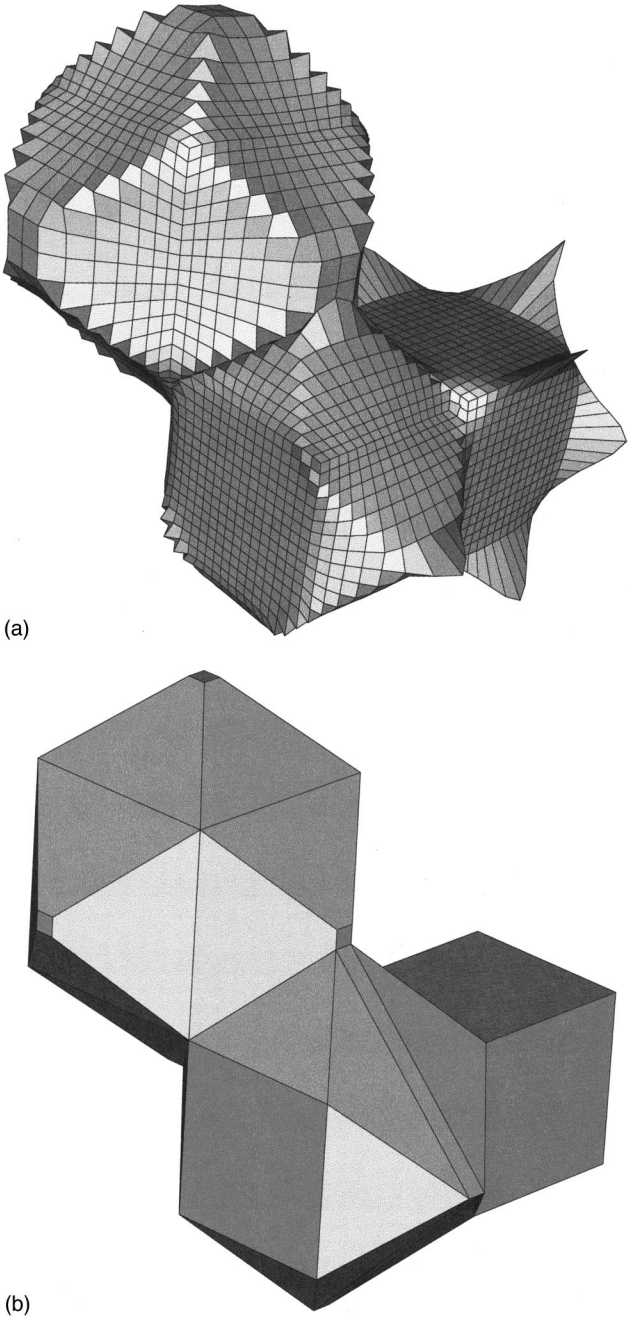

FIG. 2. Attraction basins (above) and weighted proximity polyhedra (WPP, below) for each ion in the perovskite $\mathcal{B}_{10}$ topological scheme. The basins have been computed using CRITIC (Ref. 30) and rendered using GEOMVIEW (Ref. 78). The WPP's have been obtained using ENVIRON (Ref. 79) and rendered using GEOMVIEW (Ref. 78). In each plot the A^+ ion is the uppermost figure, the M^{2+} ion is the rightmost one, and the X^- ion lies in the middle of the other two. The WPP's are described in Table IV.

edges to linear representations some fictitious facets may appear, that is, facets that are not associated to a bond point. For algorithmic simplicity we have chosen the cage points to define the vertices of the polyhedral representation, the WPP's being just the convex hull[34] defined by those vertices.

The relation between the attraction basin and the WPP is presented in Fig. 2 for the $\mathcal{B}_{10}$ topological scheme. We can see that the basin of Cs^+ is a rhombododecahedron with the acute vertices of the rhombi cut away to form new small square faces. The rhombi are associated to the Cs-F bonds, whereas the small square faces correspond to Cs-Cs bonds. The F^- basin has only six real faces: four rhombi related to Cs-F bonds, and two large and curved squares corresponding to Sr-F bonds. Within the polyhedral approximation, every curved square appears as a smaller square with four triangles connected to it by an edge each. Were they real, the triangles of the F^- basin would represent F-F bonds, which do not exist in $\mathcal{B}_{10}$. The way the structure avoids face to face contact between two neighbor F^- basins, implying an F-F bond, is that the Sr^{2+} basins develop triangular and nearly bidimensional *wings* that perfectly envelop the curved triangles of the F^- basins. Apart from those strange wings, the Sr^{2+} basin could be confounded with a slightly engrossed cube, and that is the best convex polyhedral approximation, used to plot the WPP.

The attraction basins for the ions in the $\mathcal{C}$ and $\mathcal{R}$ topological schemes have been depicted in Fig. 3. Table IV presents the number and identity of faces, edges, and vertices for each basin. Figure 4, finally, shows the associated WPP's.

The first thing to notice is that the convex WPP's are good approximations to the shape of the attraction basins in all cases except for the M^{2+} basin in $\mathcal{C}_8$ and $\mathcal{R}_9$ schemes. Faces are mostly planar, the exception being the basins of small cations when combined with large anions, which appear rather rounded and spherelike. The basin of the A^+ ions presents in the six $\mathcal{C}$ and $\mathcal{R}$ schemes the topology, and to a very good approach the geometry, of a rhombododecahedron, the 12 identical faces being related to the A-X bonds between the ion and its nearest neighbors.

The halide basins present a progressive greater complexity in passing from $\mathcal{C}_8$ to $\mathcal{R}_{13}$. The X^- basins have six faces in the $\mathcal{C}_8$ and $\mathcal{R}_9$ schemes: two axial faces associated to the M-X bonds, and four equatorial faces due to the A-X bonds. The two axial faces are very curved and appear nearly as a square with four triangles ($\mathcal{C}_8$) or four trapezoids ($\mathcal{R}_9$) glued to it at the edges. Each axial face, in fact, gives rise to five polygons in the convex WPP. The X^- basins, on the other hand, present 14 true faces in the $\mathcal{C}$ and $\mathcal{R}$ schemes with $\tau \geqslant 10$: the 6 faces previously discussed, and 8 new faces due to the X-X bonds.

From a geometrical point of view, the basins of two neighbor X^- ions do contact each other along a polygon of the WPP. Topologically, however, that polygon is a bond-related face only in the $\tau \geqslant 10$ $\mathcal{C}$ and $\mathcal{R}$ schemes. This property determines one of the most striking features depicted in Fig. 3. M^{2+} basins in $\mathcal{C}_8$ and $\mathcal{R}_9$ have the shape of a cube with nearly flat wings extending from the edges of the cube. The wings go between neighbor X^- basins, effectively avoiding them to have contact along the fictitious faces. In the case of $\mathcal{C}_{10}$ to $\mathcal{R}_{13}$, the M^{2+} basin is topologically equivalent to a cube; the basins show more or less acute spikes on the cube vertices for $\mathcal{C}_{10}$ and $\mathcal{R}_{11}$, and a round, nearly spherical, shape for $\mathcal{C}_{12}$ and $\mathcal{R}_{13}$.

To end this analysis we should stress that A^+ cations maintain a rather constant shape among crystals, whereas the anion basin stretches to fill in the gap between cations.

C. The origin of the different topological schemes

Once the different topological schemes have been described in detail, the question is what crystal exhibits which

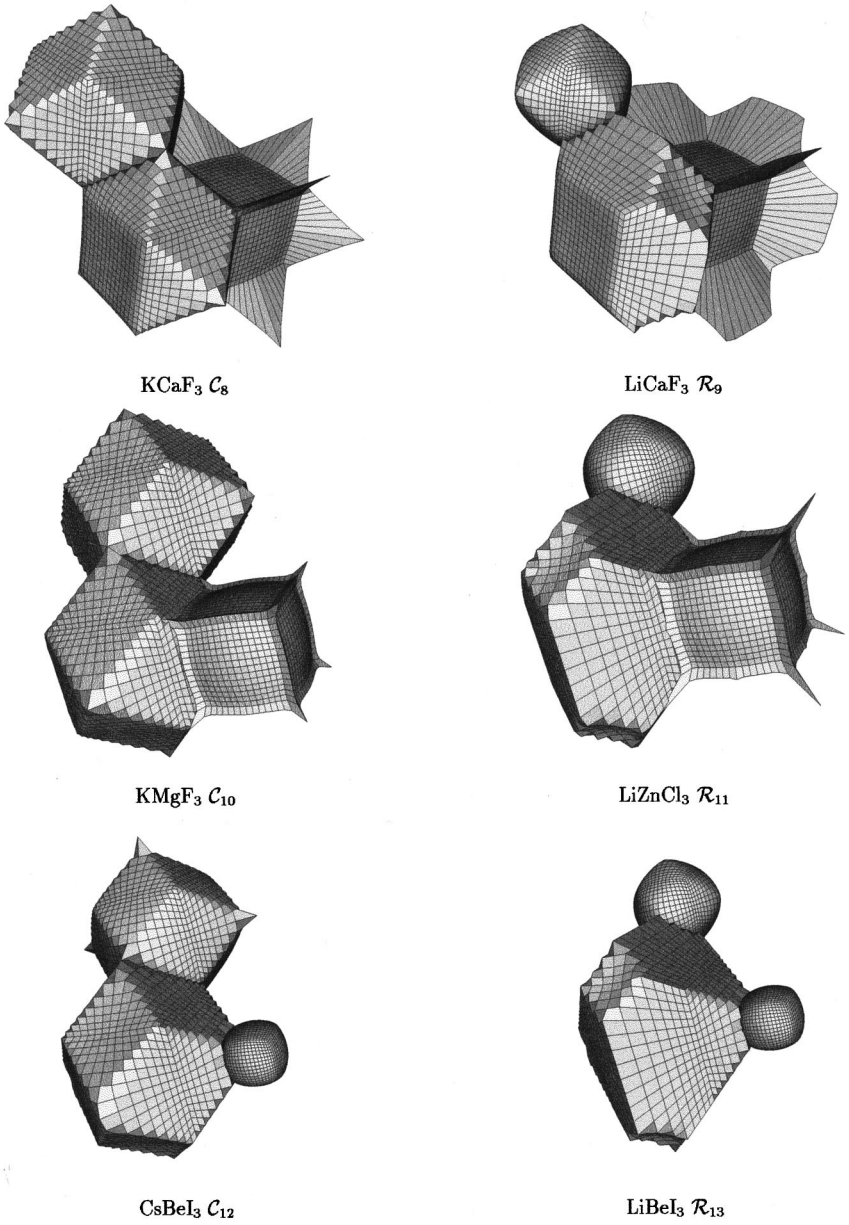

FIG. 3. Attraction basins for each ion in the $\mathcal{C}$ and $\mathcal{R}$ families of topological schemes in the perovskites. The basins have been computed using CRITIC (Ref. 30) and rendered using GEOMVIEW (Ref. 78). For each crystal the A^+ ion is the uppermost figure, the M^{2+} ion is the rightmost one, and the X^- ion lies in the middle of the other two. It is convenient to analyze this plot together with Table IV and Fig. 4.

scheme and why. In doing this analysis we will concentrate on $\mathcal{C}$ and $\mathcal{R}$ schemes, the $\mathcal{B}_{10}$ one being rare, as described before.

Topological ionic radii can be defined as the distance from the nucleus to the surface of its attraction basin. It is evident from Figs. 2 and 3 that such topological radii do depend strongly on the direction being analyzed. Not all directions are equally important, however, those containing bonds being the most significant ones for the crystal stability. In this way, the b_1 CP, which represents an M-X bond, provides estimated ionic radii for M^{2+} and X^-, which we will designate as $R(M)$ and $R_1(X)$, respectively. Similarly, the b_2 CP represents an A-X bond, and provides radii for A^+, $R(A)$, and for X^-, $R_2(X)$. The b_3 CP, found in many crystals, corresponds to an X-X bond and gives a third radius for X^-: $R_3(X)$. An extensive compilation of topological radii is available upon request.

We have found, after some initial surprise, that the ratio of ionic radii along the M-X and A-X bond lines completely determines the topological scheme exhibited by the crystal. To show this we have prepared Fig. 5, in which we have plotted the ratio $R(M)/R_1(X)$ versus the ratio $R(A)/R_2(X)$, every crystal being represented by a symbol different for each type of topological scheme.

It is observed in Fig. 5 that the $\mathcal{C}$ and $\mathcal{R}$ topological families are decided according to the value of $R(A)/R_2(X)$. If the A^+ ion is larger than about 0.88 times the X^- ion along the A-X bond line, the crystal belongs to the $\mathcal{C}$ family, and it belongs to the $\mathcal{R}$ family if the contrary is true.

The $R(M)/R_1(X)$ ratio, on the other hand, is in control of the topological complexity within each family: the larger M^{2+} is in comparison to X^-, the simpler the topological scheme appears. $\mathcal{C}_8$ and $\mathcal{R}_9$ occur for $R(M)/R_1(X) \geqslant 0.82$, $\mathcal{C}_{10}$ and $\mathcal{R}_{11}$ for $0.82 \geqslant R(M)/R_1(X) \geqslant 0.62$, and $\mathcal{C}_{12}$ and $\mathcal{R}_{13}$ for $R(M)/R_1(X) < 0.62$.

It is interesting to notice that although the topological radii behave similarly to Shannon's empirical radii,[35] only the topological values provide an exact criterion to predict the topological family.

TABLE IV. Characteristics of the attraction basins for each ion in the seven topological schemes of perovskites. Each basin is a simply connected 3D region that satisfies Euler invariance relationship: faces + vertices = edges + 2.

Crystal	Scheme	Ion	Faces	Vertices	Edges	Comments
$CsSrF_3$	$\mathcal{B}_{10}$	Cs	$12b_2+6b_4$	$8c_2+24c_5$	$24r_1+24r_5$	
		Sr	$6b_1$	$8c_2+12c_5$	$24r_1$	wings
		F	$2b_1+4b_2$	$8c_2+8c_5$	$16r_1+4r_5$	
$KCaF_3$	$\mathcal{C}_8$	K	$12b_2$	$8c_2+6c_1$	$24r_1$	
		Ca	$6b_1$	$8c_2+12c_1$	$24r_1$	wings
		F	$2b_1+4b_2$	$8c_2+4c_1$	$16r_1$	
$LiCaF_3$	$\mathcal{R}_9$	Li	$12b_2$	$8c_2+6c_3$	$24r_1$	
		Ca	$6b_1$	$8c_2+24c_3$	$24r_1+12r_2$	wings
		F	$2b_1+4b_2$	$8c_2+8c_3$	$16r_1+4r_2$	
$KMgF_3$	$\mathcal{C}_{10}$	K	$12b_2$	$8c_2+6c_1$	$24r_1$	
		Mg	$6b_1$	$8c_2$	$12r_3$	
		F	$2b_1+4b_2+8b_3$	$8c_2+4c_1$	$16r_1+8r_3$	
$LiZnCl_3$	$\mathcal{R}_{11}$	Li	$12b_2$	$8c_2+6c_3$	$24r_1$	
		Zn	$6b_1$	$8c_2$	$12r_3$	
		Cl	$2b_1+4b_2+8b_3$	$8c_2+8c_3$	$16r_1+8r_3+4r_2$	
$CsBeI_3$	$\mathcal{C}_{12}$	Cs	$12b_2$	$8c_2+6c_1$	$24r_1$	
		Be	$6b_1$	$8c_4$	$12r_3$	
		I	$2b_1+4b_2+8b_3$	$8c_2+4c_1+8c_4$	$16r_1+8r_3+8r_4$	
$LiBeI_3$	$\mathcal{R}_{13}$	Li	$12b_2$	$8c_2+6c_3$	$24r_1$	
		Be	$6b_1$	$8c_4$	$12r_3$	
		I	$2b_1+4b_2+8b_3$	$8c_2+8c_3+8c_4$	$16r_1+8r_3+4r_2+8r_4$	

Let us discuss now the bond angles observed in the different crystals, which we will determine as the angle ion-bond-ion. Symmetry fixes the M-X and A-X bond paths to be straight lines, and the bond angles to be exactly 180°. The X-X bond, when present, does not have this restriction, and the deviation of the $\alpha(X,X)$ angle from 180° provides an indication of the stress in the bond. We have found that $\alpha(X,X)$ varies from 172.30°, found in $NaZnCl_3$, to 179.98°, found in $CsMgF_3$. There is a tendency for crystals having a large $R(M)/R_1(X)$ ratio to deviate from the linearity in the X-X bond. This effect can be regarded as a step in the elimination of the X-X bond when $R(M)/R_1(X)$ increases above ≈ 0.82.

D. Atomic properties

The topological analysis offers detailed information regarding individual ions within the crystal. We will analyze here some of the most significant results found on examining two different sources of data: the geometrical position of CP's, and the properties obtained by integrating appropriate functionals over the attraction basins.

Let us analyze first the topological ionic radii. After examining the data for correlations among the size of the different ions, the clearest relationship appears between $R(M)$ and $R_1(X)$ (see Fig. 6). $R(M)$ is proportional to the radius of the halide ion and rather independent from the alkali ion size. Similar behaviors have been previously reported.[36] On the other hand, if we consider those crystals having the same A^+ and X^- but different M^{2+}, $R_1(X)$ is inversely proportional to the size of M^{2+}, although Zn^{2+} compounds fail to lie in between Mg^{2+} and Ca^{2+} as they should, according to the $R(M)$ radii.

A further perspective on the ionic properties is obtained by integrating appropriate functionals over the ionic basins.[37] Two of the simplest ionic properties, the charge and the volume, can be obtained, for instance, as

$$\mathcal{Q}(A)=Z_A-\int_{\Omega_A}\rho(\vec{r})d\vec{r}, \tag{4}$$

$$\mathcal{V}(A)=\int_{\Omega_A}d\vec{r}, \tag{5}$$

where Ω_A is the three-dimensional basin of A, $\rho(\vec{r})$ is the electronic density of the crystal, and Z_A is the atomic number of A. A convenient average ionic radius can be defined as the radius of a sphere having the same volume as the ionic basin:

$$\mathcal{R}(A)=\left[\frac{3}{4\pi}\mathcal{V}(A)\right]^{1/3}. \tag{6}$$

The integration over the ionic basins is computationally quite demanding. The algorithm implemented in the CRITIC program[30] involves sampling a number of rays defined by their (θ,ϕ) spherical coordinates. The position of the basin surface is determined along each ray, and a Gaussian quadrature is used to integrate with respect to the radial coordinate for each ray. Site symmetry is used to improve the performance of this method. A grid of $40\times40\times60$ points on (θ,ϕ,r) has been used in this work. This grid produces an accuracy better than 0.01 $Å^3$ in the integrated total volume of the cell, and better than 0.001 a.u. in the cell total charge.

To simplify the discussion we have determined charges and radii for each ion by averaging the raw integration data from all the crystals that contain the ion. Similarly, we have

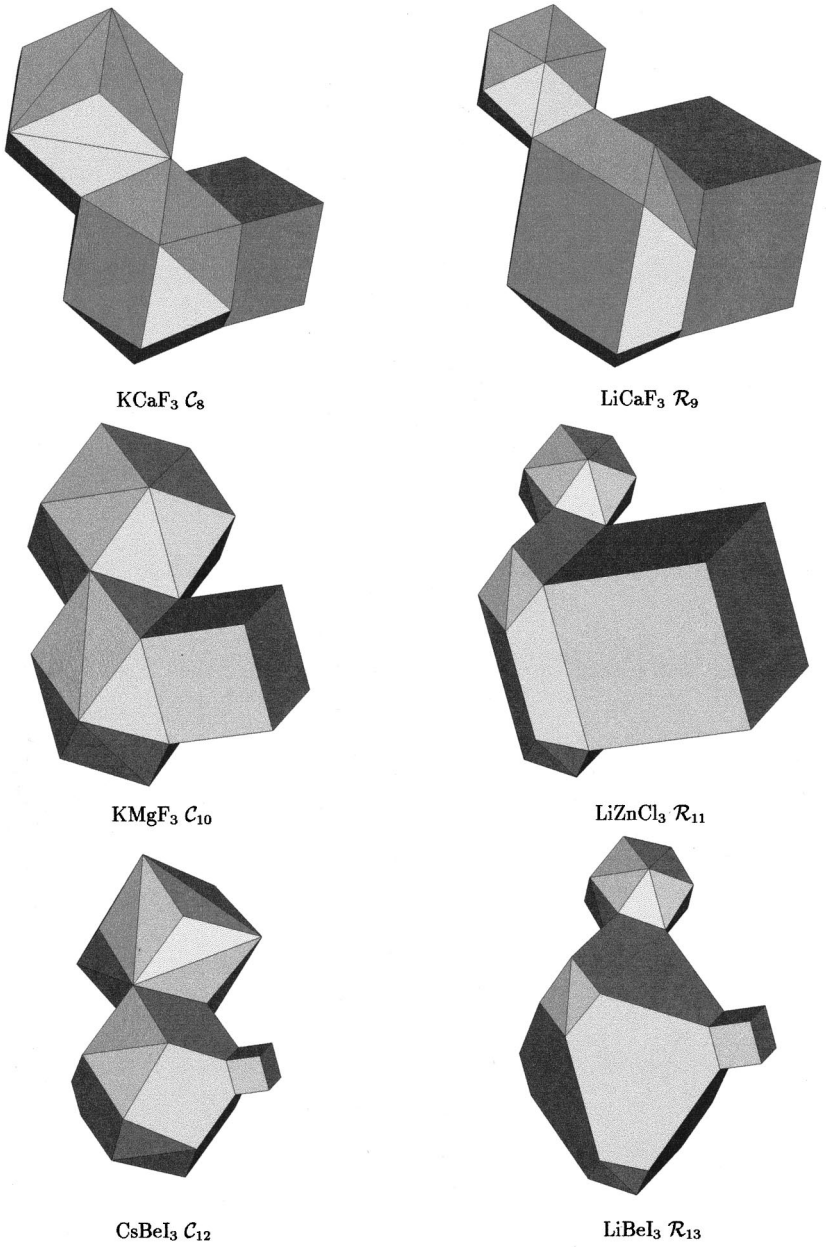

FIG. 4. Weighted proximity polyhedra (WPP) for the $\mathcal{C}$ and $\mathcal{R}$ families of topological schemes in the perovskites. The WPP's have been obtained using ENVIRON (Ref. 79) and rendered using GEOMVIEW (Ref. 78). See discussion in text.

determined the highest and lowest value of $\mathcal{Q}$ and $\mathcal{R}$ for each ion. The results of this analysis is depicted in Figs. 7 and 8.

All perovskites behave clearly as ionic compounds, as indicated by the topological charges (see Fig. 7). The charge of the alkaline ions is very close to the nominal $+1$ value, halides have an average charge $\mathcal{Q}(X)\approx -0.95$, and alkaline earth ions vary from $\mathcal{Q}(\mathrm{Be})\approx 1.95$ to $\mathcal{Q}(\mathrm{Zn})\approx 1.8$. The variability of the charge in the alkaline ions, on the other hand, increases as we descend in the Periodic Table, an effect that is observed neither on the halides nor on the alkaline earth ions.

The relative values of $\mathcal{Q}(A)$, $\mathcal{Q}(M)$, and $\mathcal{Q}(X)$ suggest a minor role of the alkali ions, as compared with the M^{2+} and X^{-} ions, in the redistribution of charge that is associated to the formation of the crystal. In other words, the A^{+} ions do not significantly participate in the formation of the chemical bond, but they have an essential contribution to the electrostatic interactions that dominates the lattice energy and, in general, the crystal energetic properties. It is also interesting to notice that the X^{-} ions donate charge to the M^{2+} ions, as is usually expected from empirical reasoning.

Several interesting effects are observed in Fig. 8. First of all, the average ionic sizes increases, within each group of ions, with the atomic number, as should be the case if we want to claim any physical meaning for $\mathcal{R}$. Second, the dispersion of ionic radii increases, within each group of ions, as we descend in the Periodic Table, following the trend of the empirical polarizabilities. With regard to the differences between groups, the alkaline earth ions present a rather constant value for $\mathcal{R}$, with the noticeable exception of Ba^{2+}, and halide ions exhibit a greater variability. The most interesting fact is, however, the large variability of radii observed for the alkaline ions, even larger than that found for the halides in sharp contradiction with the polarizabilities of both groups. This circumstance suggests that the variability of $\mathcal{R}(A)$ has a different origin than the variability of $\mathcal{R}(M)$ and $\mathcal{R}(X)$. It appears that the A^{+} ions are weakly bound within the cage made up of M^{2+} and X^{-} ions, in

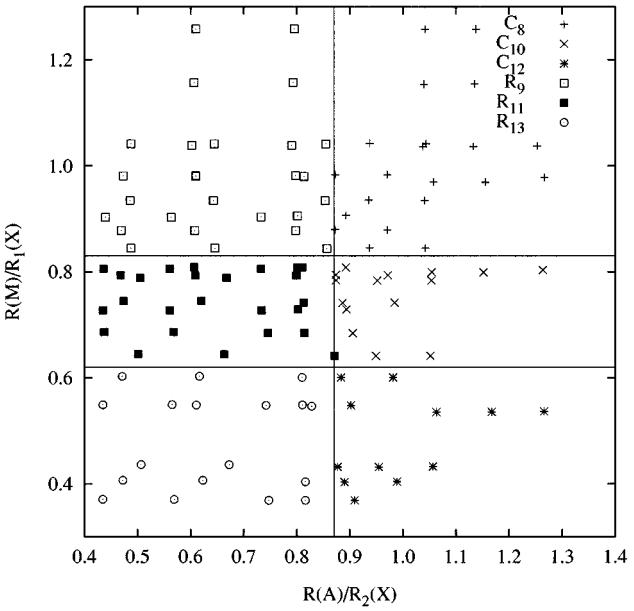

FIG. 5. Classification of the topological schemes of the perovskites and its relationship to the ionic size ratios $R(M)/R_1(X)$ and $R(A)/R_2(X)$.

agreement with the minor role of A^+ ions in the charge redistribution that was previously indicated.

E. Lattice energy

The simplest measurement of the crystal stability is provided by the lattice energy, defined as the energy of the reaction

$$AMX_{3\,(s)} \rightarrow A^+_{(g)} + M^{2+}_{(g)} + 3X^-_{(g)}\,. \tag{7}$$

We have represented in Fig. 9 the lattice energies versus the lattice parameter a of the 120 perovskites. The figure evidences that the lattice energy varies as $-\mathcal{M}/a$, the classical Madelung relationship. It is very interesting to observe that even though the lattice parameter is the result of the complicated competition between quantum and classical-like forces, once a is determined, the electrostatic interactions appear to dominate the lattice energy.

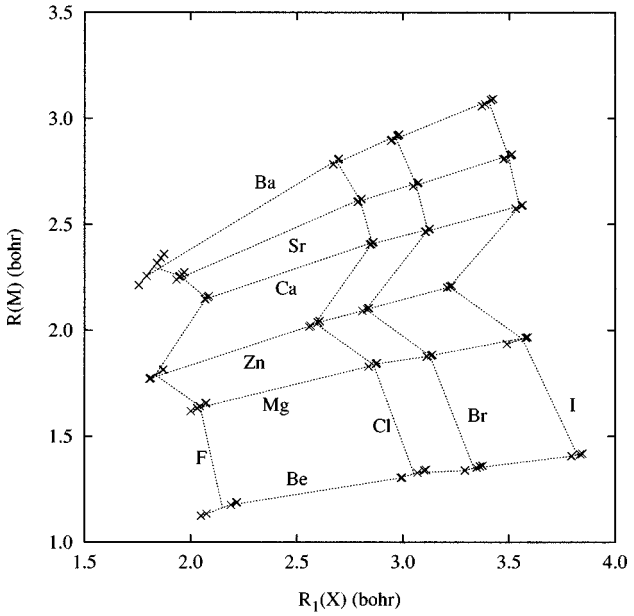

FIG. 6. Analysis of the ionic radii obtained as the geometrical distance between the ions and the bond critical points: correlation between $R(M)$ and $R_1(X)$.

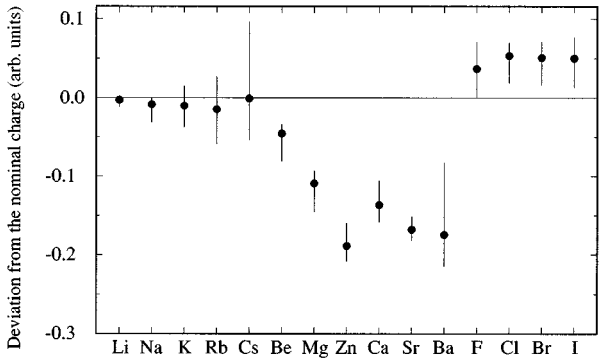

FIG. 7. Deviation of the topological ionic charges $\mathcal{Q}$ from the nominal $+1$ (A^+), $+2$ (M^{2+}), and -1 (X^-) values. The charges have been averaged to all crystals. Error bars represent the highest and lowest values among crystals.

On the other hand, we have found that varying the A^+ ion has a very small effect on the bulk crystal properties: a, E_{latt}, and B. This observation is consistent with the small role that the A^+ ions play in the redistribution of charge that is usually associated with the chemical binding. Even if this effect is small, we may observe that the lattice parameter (and the lattice energy) increases in passing from Li^+ to Na^+ to K^+ compounds, and then decreases in passing to Rb^+ and to Cs^+ compounds. This very same tendency has been found on alkali halides.

It has been previously observed, through the analysis of a series of similar compounds, that the stability of a compound correlates with the value of the electronic density at the bond CP (see, for instance, Ref. 1). Table V shows that M-X have, on average, the largest value of ρ among bonds, and should play the dominant role in deciding bond-related properties.

We have plotted in Fig. 10 the lattice energy against $\rho(b_1)$, the density at the M-X bond CP. Not surprisingly, each different combination of M and X appears in a different region of the diagram, but the figure also shows that the lattice energies of those crystals having M in common are

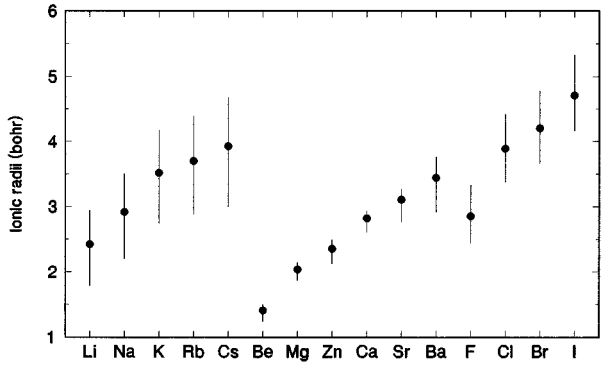

FIG. 8. Ionic radii $\mathcal{R}$ obtained from the volume of the attraction basins and averaged to all crystals. Error bars represent the highest and lowest values among crystals.

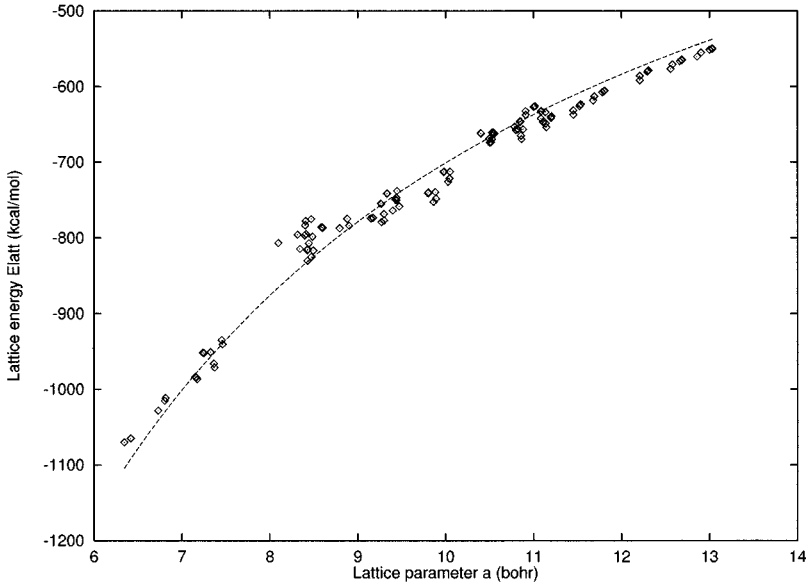

FIG. 9. Correlation between the lattice energy and the unit cell side length. The broken line represents the best fit to the equation: $E_{\mathrm{latt}} = -\mathcal{M}/a$ ($\mathcal{M} = 7007 \pm 17$ bohr kcal/mol $= 11.167 \pm 0.027$ a.u.). The best fit parameter can be compared to the electrostatic Madelung constant of perovskites: 12.377468 a.u. (7766.99 bohr kcal/mol).

essentially proportional to $\rho(b_1)^{1/3}$. Even though the electrostatic interaction appears to dominate the lattice energy, the bond strength, represented by $\rho(b_1)$, has a clear influence too.

IV. DISCUSSION AND CONCLUSIONS

Nuclei act as attractors in the electronic density gradient fields. Moreover, very few examples of non-nuclear attractors have been reported so far[38–40] and none has been found in our study of the perovskites. Since the topological structure and stability are determined as a result of the balance between the attractors of the system, we should anticipate a significant degree of similarity in the topological properties of the AMX_3 perovskites. The rich variety of topological schemes found is, in this regard, an interesting surprise. Our study has shown that the organizing principle behind that variety is the ratio between topological ionic radii along the main bond paths or, in other words, the competition between atomic basins to achieve a kind of preferred size.

Ionic radii along the bond paths follow systematic trends in passing from one crystal to another, even though the ionic radius of an ion in a crystal strongly depends on the direction being considered.

Contrary to the common wisdom of assuming spherical ions, ionic basins have, essentially, a polyhedral shape, even though faces and edges present very large curvatures in some cases. Each bond CP acts as an attractor for a set of points lying in a bidimensional sheet, thus being the origin of a face or limiting surface of the two ionic basins that the CP binds together. Similarly, each ring CP is the attractor for the points in a line and originates an edge between several ionic basins. Cage CP's, finally, are repulsion centers for the gradient field lines in all directions and provide the vertices of the ionic basins. The type and number of CP's in the unit cell are limited by the Morse invariant relationships. The type and number of CP's in the surface of an ionic basin are limited by the Euler relation. Both conditions, together with the space-group symmetry, put strict requirements on the shape of the ionic basins. This point of view helps to explain some of the bizarre features exhibited by the basins in some cases, particularly the nearly bidimensional wings of the M^{2+} basins in the $\mathcal{C}_8$, $\mathcal{R}_9$, and $\mathcal{B}_{10}$ topological schemes.

One of our objectives when we started this study was to determine whether the stability of the crystal is correlated or not with the topological structure. The lattice energy, which measures the difficulty in breaking apart the crystal into its isolated ions, is dominated by the electrostatic interactions and follows the simple a^{-1} Madelung law. Grouping together the crystals that have the same M^{2+} cation, we also observed, as a secondary effect, that E_{latt} is proportional to $\rho(b_1)^{1/3}$, where $\rho(b_1)$ is the value of the electronic density in the M-X bond CP.

On a more fundamental basis, the stability of the crystal should be addressed with respect to (a) solid-state reactions producing compounds of different stoichiometry, and (b) the existence of crystals with the same AMX_3 stoichiometry but a different crystalline structure. To our knowledge, there is neither experimental nor theoretical data regarding the chemical stability of perovskites but for a handful of the compounds studied in this work.

$RbCaF_3$ is the best studied of the perovskites analyzed in this work, both from the experimental[41–55] and theoretical[56–60] points of view. The perovskite structure is stable above ~ 193 K; below this temperature the crystal is

TABLE V. Average values of the electronic density (in units of 10^{-3} bohr^{-3}) at the bond CP's. Bonds are labeled as in Table III: b_1 is the M-X bond, b_2 the A-X, b_3 the X-X, and b_4 the A-A bond.

Crystals	$\rho(b_1)$	$\rho(b_2)$	$\rho(b_3)$	$\rho(b_4)$
$\mathcal{B}_{10}$	84.681	12.938		1.740
$\mathcal{C}_8$	42.917	6.207		
$\mathcal{R}_9$	35.426	0.750		
$\mathcal{C}_{10}$	25.824	10.469	8.516	
$\mathcal{R}_{11}$	21.749	1.316	6.943	
$\mathcal{C}_{12}$	12.451	11.684	12.475	
$\mathcal{R}_{13}$	13.076	2.806	13.156	
All	27.970	4.632	9.770	1.740

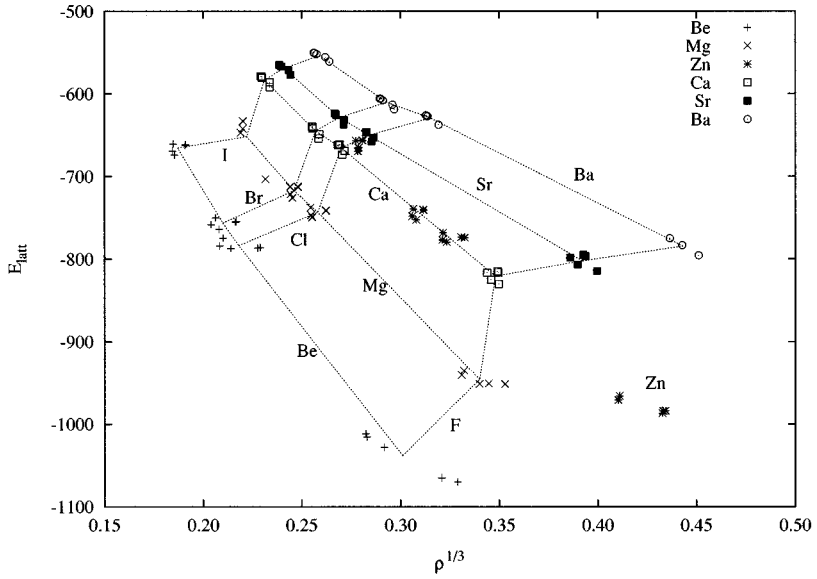

FIG. 10. Relationship between the lattice energy and the value of the electronic density at the M-X bond critical point.

most stable as a tetragonal ($I4/mcm$) phase in the range 50–193 K, as an orthorhombic ($Pnma$) phase in the range 10–50 K, and there are evidences of a different (possibly monoclinic) phase below ~10 K. $NaMgF_3$ (Refs. 61 and 62) presents similar phase transitions. The low symmetry phases have been categorized as the result of tilting the MX_6 coordination octahedra about one, two, or three independent axes.[63–67,56] These studies suggest that the high-symmetry perovskite phase can be regarded as the dynamical average of lower-symmetry tilted-octahedra structures. The relationship between phase transitions and topological structure of ρ, albeit very interesting, is beyond the scope of this work.

On the other hand, perovskites are usually prepared by melting together MX_2 and AX in 1:1 stoichiometric proportions and slowly cooling while the AMX_3 crystal is simultaneously grown and extracted according to the Czochralski procedure (see, for instance, Ref. 68). Even though, to the best of our knowledge, there is no systematic study on the energetics of the above reaction, most of the 120 AMX_3 compounds have never been referred to in the literature, which suggests that most of the perovskites are unstable with respect to MX_2+AX.

To address this problem we have determined the energy of the reaction

$$MX_{2\,(s)}+AX_{(s)}\rightarrow AMX_{3\,(s)} \tag{8}$$

as

$$\Delta E=E(AMX_3)-E(MX_2)-E(AX), \tag{9}$$

where E(compound) is the *ai*PI total energy of the crystal. The optimum geometries and energies have been used for the AMX_3 compounds. The fluorite structure [cubic, $Fm3m$, M^{2+} at (0,0,0), X^- at (1/4,1/4,1/4)] has been assumed for the MX_2 compounds, and the rock-salt structure has been assumed for the AX compounds. Even though perovskite, fluorite, and rock-salt are not necessarily the most stable structures of the three types of compounds, the difference should not be very large nor should it modify the general trends for the whole set of crystals.

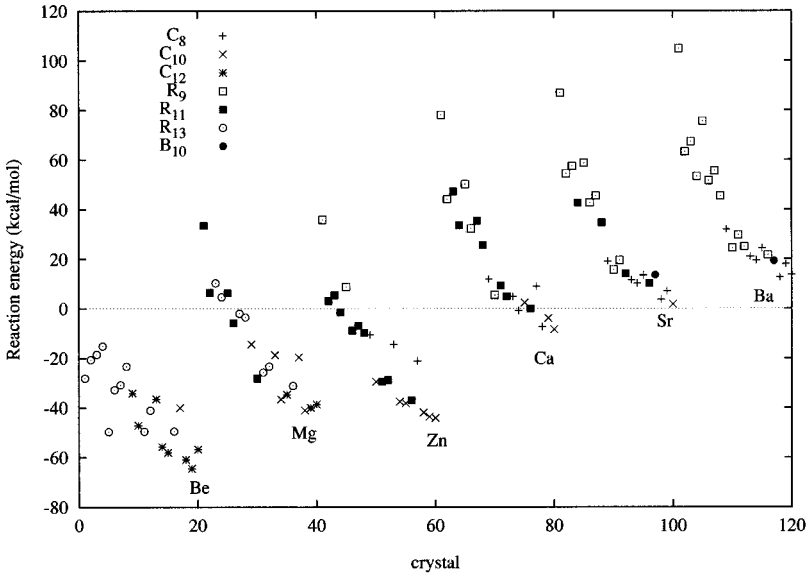

FIG. 11. Stability of the perovskite structure with respect to reaction (8). Different symbols are used for each topological scheme. Negative reaction energies imply the perovskite being stable. Crystals are ordered in such a way that compounds with a common M^{2+} are together and, within them, those having the same A^+ are next to each other. In other words, the ordering scheme is $\{M[A(X)]\}$, the innermost element varying the quickest.

Figure 11 represents the reaction energy of Eq. (8) together with the topological scheme for the 120 AMX_3 compounds. The first thing to notice is that the crystal stability is dominated by the identity of the M^{2+} cation: Ba^{2+}, Sr^{2+}, and most Ca^{2+} perovskites are unstable, whereas most Zn^{2+} and Mg^{2+} and all Be^{2+} perovskites are stable. For a given M^{2+}, stability is favored by having large A^+ ions. The role of X^- is more complex, but it is seen that fluorides are different from the other halides, either more stable or less, the chlorides, bromides, and iodides displaying rather similar behavior.

It is very interesting to observe in Fig. 11 that all crystals having $\mathcal{R}_9$ and $\mathcal{B}_{10}$, and most crystals having $\mathcal{C}_8$ topological scheme, are unstable. Contrarily, all $\mathcal{C}_{12}$ and most $\mathcal{R}_{13}$ crystals are stable. It appears that the existence of bizarre features, such as wings, in the attraction basins works against the stability of the crystal. Alternatively, we can argue that the formation of X-X bonds is important to stabilize the structure. This sheds new light on the question of what is simple and what is complex in relation to the topological structure of ρ. The simple enumeration of critical points would suggest that those topological schemes having the smallest values for τ are the simplest ones. The shape of the attraction basins is simpler, however, in the schemes of large τ and, as the analysis of reaction (8) indicates, those schemes are more favored in energetic terms.

This suggestive connection between the topological properties of the electronic density and the chemical stability of perovskites is in agreement with previous results relating the stability of the $B1$ and $B2$ phases of the alkali halides to the ratio of ionic radii obtained through topological arguments.[69]

We have also studied reaction (8) with respect to the formation of antiperovskites instead of perovskites. Antiperovskites, MAX_3, have the same structure as perovskites, except that M^{2+} and A^+ exchange their position. A^+ ions are octahedrally coordinated by the anions and the A-X bonds will dominate. According to our results, the only antiperovskites that are simultaneously more stable than the perovskite and MX_2+AX are $CaLiF_3$, $SrLiF_3$, and $BaLiF_3$. Even more, the perovskite structure should be unstable in the three compounds. $BaLiF_3$ is the only antiperovskite experimentally observed among the AMX_3 compounds.[68,70,71] However, we have found no mention whatsoever to neither $Li_mCa_nF_x$ nor $Li_mSr_nF_x$ compounds in the literature or the crystallographic databases, thus leaving the possibility that stable $CaLiF_3$ and $SrLiF_3$ antiperovskites have been simply missed up to now.

The above results refer to the difference between quantum-mechanical total energies. They correspond, thermodynamically, to null temperature and pressure. We have investigated the role of thermal effects, up to about 900 K, on the perovskite stability and have found interesting but small effects that do not modify the general trends discussed above. A detailed discussion of our calculations will be presented elsewhere.[72]

The crystal side length can be largely modified by the application of external pressure or, to a more limited extent, by heating the crystal. It is interesting to know up to which point such external perturbations can influence the topological structure of the electron density. Calculations done on the alkali halides evidence that the ionic properties and the position of the CP's do present a smooth variation with respect to the crystal side length a, but the topological scheme found at the equilibrium geometry is maintained for a wide range of a values. This behavior is related to the fact that ionic radii change linearly with a, but their ratios remain essentially constant. This observation does not preclude the existence of a change in the topological scheme induced by the change of a, but it can be regarded as a rare possibility.

To end this work we want to stress the importance and usefulness of the atoms in molecules theory as a tool to analyze and describe the properties of a solid. Rather than empirically inventing arbitrary recipes, AIM theory gives a rigorous foundation to important historical concepts such as ionicity, index of coordination, coordination polyhedra, volume of an atom in a solid, and many more. Of great importance is to observe that AIM theory does not rely on any approximation to introduce such concepts but, in fact, topologically defined properties would improve as a consequence of any improvement in the wave function.

ACKNOWLEDGMENTS

We are grateful to the Centro de Cálculo Científico of the University of Oviedo for computational facilities. Financial support from the Spanish Dirección General de Investigación Científica y Técnica (DGICYT), Project No. PB93-0327, is also acknowledged.

[1] R. F. W. Bader, *Atoms in Molecules* (Oxford University Press, Oxford, 1990).
[2] R. F. W. Bader, T. T. Nguyen-Dang, and Y. Tal, Rep. Prog. Phys. **44**, 893 (1981).
[3] P. Zou and R. Bader, Acta Crystallogr. A **50**, 714 (1994).
[4] V. Tsirelson, P. Zou, T. Tang, and R. Bader, Acta Crystallogr. A **51**, 143 (1995).
[5] M. Eberhart, M. Donovan, J. MacLaren, and D. Clougherty, Prog. Surf. Sci. **36**, 1 (1991).
[6] M. Eberhart, M. Donovan, and R. Outlaw, Phys. Rev. B **46**, 12 744 (1992).
[7] M. Eberhart, J. MacLaren, and D. Clougherty, J. Mater. Res. **8**, 438 (1993).
[8] C. Mei, K. Edgecombe, V. Smith, and A. Heilingerbrunner, Int. J. Quantum Chem. **48**, 287 (1993).
[9] G. Grosch, B. Freytag, K. Range, and U. Rösler, J. Chem. Phys. **101**, 6782 (1994).
[10] C. Johnson (unpublished).
[11] R.W.F. Bader's Laboratory, *AIMPAC* (1989).
[12] A. M. Pendás, A. Costales, and V. Luaña, preceding paper, Phys. Rev. B **55**, 4275 (1997).
[13] V. Luaña and L. Pueyo, Phys. Rev. B **41**, 3800 (1990).
[14] V. Luaña, A. M. Pendás, J. M. Recio, E. Francisco, and M. Bermejo, Comput. Phys. Commun. **77**, 107 (1993).
[15] E. Francisco, A. M. Pendás, and W. H. Adams, J. Chem. Phys. **97**, 6504 (1992).
[16] R. McWeeny, *Methods of Molecular Quantum Mechanics*, 2nd ed. (Academic, London, 1992).

[17] S. Huzinaga, D. M. Williams, and A. A. Cantú, Adv. Quantum Chem. **7**, 187 (1973).
[18] W. H. Adams, J. Chem. Phys. **34**, 89 (1961).
[19] T. L. Gilbert, in *Molecular Orbitals in Chemistry, Physics and Biology*, edited by P. O. Löwdin and B. Pullman (Academic, New York, 1964).
[20] J. M. Recio, A. M. Pendás, E. Francisco, M. Fórez, and V. Luaña, Phys. Rev. B **48**, 5891 (1993).
[21] A. M. Pendás, V. Luaña, J. M. Recio, M. Fórez, E. Francisco, M. A. Blanco, and L. N. Kantorovich, Phys. Rev. B **49**, 3066 (1994).
[22] A. M. Pendás, J. M. Recio, M. Flórez, V. Luaña, and M. Bermejo, Phys. Rev. B **49**, 5858 (1994).
[23] V. Luaña, J. M. Recio, and L. Pueyo, Phys. Rev. B **42**, 1791 (1990).
[24] R. Franco, J. Recio, A. Martín Pendás, V. Luaña, and L. Pueyo, in *New Challenges in Computational Quantum Chemistry*, edited by R. Broer, P. J. C. Aerts, and P. S. Bagus (Groningen University, Groningen, 1994).
[25] R. Franco, M. A. Blanco, A. Martín Pendás, E. Francisco, and J. M. Recio, Solid State Commun. **98**, 41 (1996).
[26] J. Andrés and A. Beltrán, Chem. Phys. Lett. **221**, 249 (1994).
[27] J. M. Recio, R. Pandey, and V. Luaña, Phys. Rev. B **47**, 3401 (1993).
[28] E. Clementi and C. Roetti, At. Data Nucl. Data Tables **14**, 177 (1974).
[29] S. Chakravorty and E. Clementi, Phys. Rev. A **39**, 2290 (1989).
[30] A. M. Pendás, THE CRITIC PROGRAM, 1995. The code is available from the authors upon request. Electronic address: angel@fluor.quimica.uniovi.es
[31] M. Morse and S. S. Cairns, *Critical Point Theory in Global Analysis and Differential Geometry* (Academic Press, New York, 1969).
[32] W. Jones and N. H. March, *Theoretical Solid State Physics* (Dover, New York, 1985), Vol. 1.
[33] L. Pauling, *The Nature of Chemical Bond* (Cornell University Press, Ithaca, NY, 1960).
[34] J. O'Rourke, *Computational Geometry in C* (Cambridge University Press, Cambridge, 1994).
[35] R. D. Shannon, Acta Crystallogr. B **32**, 751 (1976).
[36] S. Feth, G. Gibbs, M. Boisen, and R. Myers, J. Phys. Chem. **97**, 11 445 (1993), and references therein.
[37] R. F. W. Bader, Phys. Rev. B **49**, 13 348 (1994).
[38] C. Gatti, P. Fantucci, and G. Pacchioni, Theor. Chim. Acta **72**, 433 (1987).
[39] J. Cioslowski, J. Phys. Chem. **94**, 5496 (1990).
[40] R. Glaser, R. Waldron, and K. Wiberg, J. Phys. Chem. **94**, 7357 (1990).
[41] F. Modine, E. Sonder, W. Unruh, C. Finch, and R. Westbrood, Phys. Rev. B **10**, 1623 (1974).
[42] W. Kamitakahara and C. Rotter, Solid State Commun. **17**, 1350 (1975).
[43] C. Ridou, M. Rousseau, J. Gesland, J. Nouet, and A. Zarembowitch, Ferroelectrics **12**, 199 (1976).
[44] M. Rousseau, J. Nouet, and R. Almairac, J. Phys. (Paris) **38**, 1423 (1977).
[45] A. Bulou, C. Ridou, M. Rousseau, J. Nouet, and A. Hewat, J. Phys. (Paris) **41**, 87 (1980).
[46] H. Jex, J. Maetz, and M. Mullner, Phys. Rev. B **21**, 1209 (1980).
[47] C. Ridou, M. Rousseau, and J. Bouillot, Ferroelectrics **36**, 463 (1981).
[48] M. Rousseau, C. Ridou, and A. Bulou, Solid State Commun. **12**, 951 (1982).
[49] P. Simon, J. Rousseau, and J. Buzare, J. Phys. C **15**, 5741 (1982).
[50] T. Ryan, R. Nelmes, R. Cowley, and A. Gibaud, Phys. Rev. Lett. **56**, 2704 (1986).
[51] C. Ridou, M. Rousseau, and F. Gervais, J. Phys. C **19**, 5757 (1986).
[52] A. Gibaud, T. Ryan, and R. Nelmes, J. Phys. C **20**, 3833 (1987).
[53] A. Gibaud, R. Cowley, and P. Mitchell, J. Phys. C **20**, 3849 (1987).
[54] M. Hepp, P. Man, A. Trokiner, H. Zanni, and J. Fraissard, Solid State Commun. **84**, 869 (1992).
[55] M. Krupski and J. Buzare, J. Phys. Condens. Matter **6**, 9429 (1994).
[56] M. Rousseau, A. Bulou, C. Ridou, and A. Hewat, Ferroelectrics **25**, 447 (1980).
[57] L. Boyer and J. Hardy, Phys. Rev. B **24**, 2577 (1981).
[58] J. Flocken, R. Guenther, J. Hardy, and L. Boyer, Phys. Rev. B **31**, 7252 (1985).
[59] J. Flocken, R. Guenther, J. Hardy, and L. Boyer, Phys. Rev. Lett. **56**, 1738 (1986).
[60] S. Nose and M. Klein, J. Chem. Phys. **90**, 5005 (1989).
[61] Y. Zhao, D. Weidner, J. Parise, and D. Cox, Phys. Earth Planet. Inter. **76**, 1 (1993).
[62] Y. Zhao, D. Weidner, J. Parise, and D. Cox, Phys. Earth Planet. Inter. **76**, 17 (1993).
[63] A. Glazer, Acta Cryst. B **28**, 3384 (1972).
[64] A. Glazer, Acta Cryst. A **31**, 756 (1975).
[65] K. Aleksandrov, Ferroelectrics **16**, 801 (1976).
[66] K. Aleksandrov, Ferroelectrics **20**, 61 (1978).
[67] M. Rousseau, J. Phys. (Paris) **40**, L439 (1979).
[68] S. Baldochi, V. Mazzocchi, C. Parente, and S. Morato, MRS Bull. **29**, 1321 (1994).
[69] A. Martín Pendás, V. Luaña, J. Recio, M. Blanco, E. Francisco, and M. Flórez, in *First Electronic Computational Chemistry Conference (ECCC), 1994*, edited by S. M. Bachrach, D. B. Boyd, W. Hase, S. K. Gray, and H. S. Rzepa (ARInternet, 1994), paper 57.
[70] A. Boumriche, J. Gesland, A. Bulou, M. Rousseau, J. Fourquet, and B. Hennion, Solid State Commun. **91**, 125 (1994).
[71] M. Duarte, M. Vieira, and S. Baldochi, Mater. Sci. Eng. B **25**, 133 (1994).
[72] V. Luaña, A. Costales, and A. Martín Pendás (unpublished).
[73] W. Massa and D. Babel, Chem. Rev. **88**, 275 (1988).
[74] C. Ridou, M. Rousseau, J. Bouillot, and C. Vettier, J. Phys. C **17**, 1001 (1984).
[75] B. Lutger and D. Babel, Z. Anorg. Allg. Chem. **616**, 133 (1992).
[76] H. Seifert and J. Vebach, J. Solid State Chem. **59**, 86 (1985).
[77] P. Kraulis, J. Appl. Cryst. **24**, 946 (1991).
[78] M. Phillips, T. Munzner, and S. Levy, GEOMVIEW, 1995, available via anonymous ftp from geom.umn.edu (The Geometry Center at the University of Minnesota).
[79] V. Luaña, The ENVIRON program, 1995. The code is available from the authors upon request. Electronic address: victor@carbono.quimica.uniovi.es